JOURNAL OF GEOPHYSICAL RESEARCH, VOL. 115, C02002, doi:10.1029/2009JC005633, 2010

Comparison between observations and models of the Mozambique Channel transport: Seasonal cycle and eddy frequencies

P. M. van der Werf,[1] P. J. van Leeuwen,[1,2] H. Ridderinkhof,[3] and W. P. M. de Ruijter[1]

Received 10 July 2009; revised 31 August 2009; accepted 15 October 2009; published 3 February 2010.

[1] A time series of the observed transport through an array of moorings across the Mozambique Channel is compared with that of six model runs with ocean general circulation models. In the observations, the seasonal cycle cannot be distinguished from red noise, while this cycle is dominant in the transport of the numerical models. It is found, however, that the seasonal cycles of the observations and numerical models are similar in strength and phase. These cycles have an amplitude of 5 Sv and a maximum in September, and can be explained by the yearly variation of the wind forcing. The seasonal cycle in the models is dominant because the spectral density at other frequencies is underrepresented. Main deviations from the observations are found at depths shallower than 1500 m and in the 5/*y*–6/*y* frequency range. Nevertheless, the structure of eddies in the models is close to the observed eddy structure. The discrepancy is found to be related to the formation mechanism and the formation position of the eddies. In the observations, eddies are frequently formed from an overshooting current near the mooring section, as proposed by Ridderinkhof and de Ruijter (2003) and Harlander et al. (2009). This causes an alternation of events at the mooring section, varying between a strong southward current, and the formation and passing of an eddy. This results in a large variation of transport in the frequency range of 5/*y*–6/*y*. In the models, the eddies are formed further north and propagate through the section. No alternation similar to the observations is observed, resulting in a more constant transport.

Citation: van der Werf, P. M., P. J. van Leeuwen, H. Ridderinkhof, and W. P. M. de Ruijter (2010), Comparison between observations and models of the Mozambique Channel transport: Seasonal cycle and eddy frequencies, *J. Geophys. Res.*, *115*, C02002, doi:10.1029/2009JC005633.

1. Introduction

[2] In the Mozambique Channel, several water masses converge. The strength of the transport in the channel is controlled by the inflow of the Indonesian Throughflow, the Tasman Strait throughflow, and the strength of the tropical and subtropical gyre in the Indian Ocean [*Schott et al.*, 2009] (Figure 1). The Mozambique Channel is one of the main source areas of the Agulhas Current [*de Ruijter et al.*, 2005; *Schott et al.*, 2009]. This current is an important conduit in the global thermohaline circulation, as this is the route via which warm, salty Indian Ocean water enters the South Atlantic and potentially influences the Atlantic meridional overturning circulation [*Gordon*, 1986; *Schott and McCreary*, 2001; *Schouten et al.*, 2002; *Matano et al.*, 2002; *de Ruijter et al.*, 2005; *Biastoch et al.*, 2008b]. *Van Sebille et al.* [2009] found in a high-resolution model that this leakage is enhanced when the Agulhas Current is weaker, although when the far field is changed, a weaker Agulhas Current can also lead to a smaller leakage [*Franzese et al.*, 2009; *Rouault et al.*, 2009]. The mean and variability of the transport through the Mozambique Channel are therefore important quantities to monitor the system.

[3] In the past, many estimates of the mean transport have been made. Estimates, based on hydrographic data, varied between 5 Sv northward and 26 Sv southward [*DiMarco et al.*, 2002]. *Ridderinkhof and de Ruijter* [2003] found a mean transport of 14 Sv from a mooring array covering 19 months in 2000 and 2001. Experiments conducted with numerical models obtained similar results [*Biastoch and Krauss*, 1999; *Biastoch et al.*, 1999; *Matano et al.*, 2002].

[4] Most numerical models simulate a dominant seasonal cycle in the Mozambique Channel transport. For example, *Biastoch et al.* [1999] calculated a seasonal cycle with an amplitude of 10 Sv and a minimum transport of 4 Sv northward in February–March. The seasonal cycle found by *Matano et al.* [2002] had an amplitude of 6 Sv and a minimum transport in February. On the other hand, in most observational data [*Swallow et al.*, 1988; *Schott et al.*, 1988; *Ffield et al.*, 1997; *Ridderinkhof and de Ruijter*, 2003; *Schouten et al.*, 2003], no clear seasonal cycle was observed in the transport.

[5] In this study, we address this seeming discrepancy between observations and models. We use new data from both observations and numerical models that have become

[1]Institute for Marine and Atmospheric Research Utrecht, Department of Physics and Astronomy, Utrecht University, Utrecht, Netherlands.
[2]Department of Meteorology, University of Reading, Reading, UK.
[3]Royal Netherlands Institute for Sea Research, Texel, Netherlands.

0148-0227/10/2009JC005633$09.00

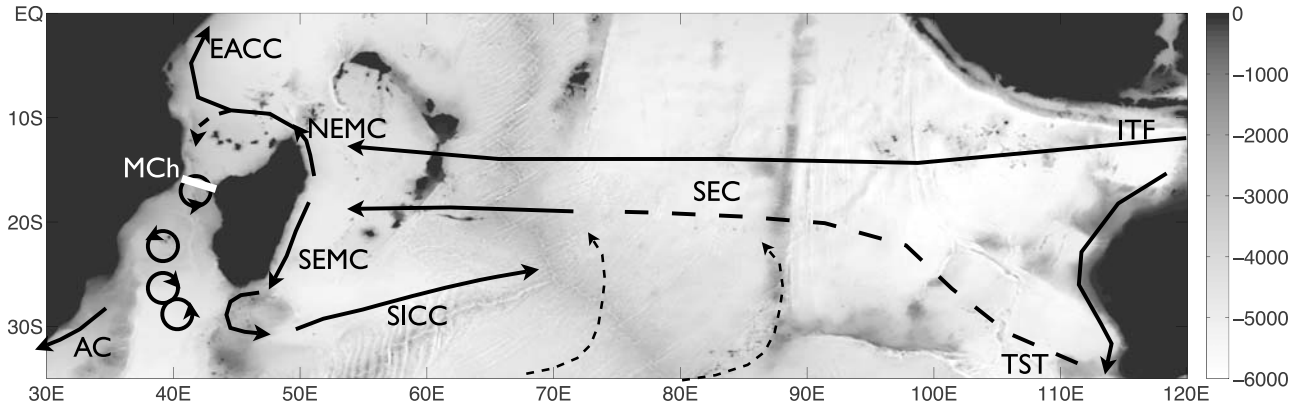

Figure 1. Depth of the Southern Indian Ocean (in meters) overlaid with the main currents. The South Equatorial Current (SEC) is fed by the Indonesian Throughflow (ITF), the Tasman Strait throughflow (TST), and the strength of the tropical and subtropical gyres. It bifurcates at the Madagascar coast into the North East Madagascar Current (NEMC) and the South East Madagascar Current (SEMC). The NEMC bifurcates again at the African coast into the northward flowing East African Coastal Current (EACC) and a flow through the Mozambique Channel (MCh), which appears as a train of eddies. Part of the SEMC retroflects back into the Indian Ocean via the South Indian Ocean Counter Current (SICC). The other part meets with the MCh throughflow into the Agulhas Current (AC). The white line in the MCh marks the LOCO mooring section.

available recently (section 2). Since November 2003, an array of moorings is being maintained across the narrowest section of the Mozambique Channel, around 16.5°S as part of the Dutch Long-Term Ocean Climate Observations (LOCO) program (see Figure 1 for its location) [*Ridderinkhof and de Ruijter*, 2003; *Harlander et al.*, 2009; *Ridderinkhof et al.*, 2010]. This mooring array contains, among others, continuous velocity measurements. Previous studies to this data set have shown that the flow across the section is dominated by anticyclonic eddies that are related to standing Rossby waves [*Ridderinkhof and de Ruijter*, 2003; *Harlander et al.*, 2009]. In addition, the transport was found to be highly variable, also at long time scales [*Ridderinkhof et al.*, 2010]. In the present study, we use velocity measurements from November 2003 to January 2008. This long time span, together with the high time resolution of the observations, gives a good measurement of the variability in a range of frequencies. The observational transport time series is compared to the output of six runs with four ocean general circulation models (OGCMs) that have a range in horizontal resolution and simulation duration. We have concentrated on the mean transport, the total transport variability, and variability in selected frequency bands, such as the seasonal cycle (section 3).

[6] Our research shows that the seasonal cycles in the numerical models have the same amplitude and phase as the seasonal cycle in the observations. However, because of the underrepresentation of the power at other frequencies, the seasonal signal dominates in the models.

[7] The actual question should therefore be why the power at other frequencies is not well simulated. Our focus will be at the $5/y-6/y$ frequency range, which is associated with the Mozambique Channel eddies and Rossby waves in the channel [*Schouten et al.*, 2003; *Harlander et al.*, 2009], and has a dominant signal in the observation transport time series (section 4). In section 5, the sensitivity of the results to the data sets will be discussed, and conclusions are drawn in section 6.

2. Data

2.1. Observational Data From LOCO and AVISO

[8] In the LOCO program, the mass and heat transport across the Mozambique Channel is being measured at its narrowest section, around 16.5°S–17°S (for its location, see Figure 1). The mooring array is a refinement of the pilot experiment that took place between 2000 and 2002 [*Ridderinkhof and de Ruijter*, 2003]. It contains temperature-salinity-depth sensors, recording current meters (RCMs), acoustic Doppler current profilers (ADCPs), and a sediment trap. In this study, only data from the RCMs and ADCPs are used.

[9] The time series consists of three periods between which the instruments were serviced and redeployed: November 2003–February 2005, March 2005–March 2006, and March 2006–January 2008. To remove tidal and inertial variability, the data were low-pass filtered (forward and backward) with a 3.5 day Butterworth filter, and subsampled at daily intervals. The data were inter- and extrapolated vertically and horizontally to obtain the transport. A full-slip boundary condition was applied at the bottom and sidewalls of the channel. *Ridderinkhof et al.* [2010] give a more elaborate discussion on the data processing. Amongst other things, they show that the transport time series is not very sensitive to the inter- and extrapolation scheme used.

[10] Sea surface height anomaly (SSHA) data were produced by Ssalto-Duacs and distributed by Archiving, Validation, and Interpretation of Satellite Oceanographic (AVISO), with support from the Centre National d'Etudes Spatiales, Toulouse, France (CNES). It was downloaded from www.aviso.oceanobs.com/en/data/products/sea-surface-

Table 1. Model Parameters

	LOCO	ECCO	ORCA025	AG01-R	OCCAM025	OCCAM008	OFES
Period	2003–2008	1993–2008	1968–2001	1968–2005	1993–2004	1993–2004	2000–2006
Span (years)	4.14	15	33	37	12	12	7
Time resolution (days)	1	10	5	5	5	5	3
Horizontal resolution (°)	-	1	0.25	0.1[a]	0.25	0.08	0.1
Grid size 16.5°S (km)	-	106.9	26.7	10.7	26.7	8.9	10.6
Total layers	-	37	32	32	47	47	43
0–100 m	-	10	10	10	14	14	14
100–500 m	-	14	9	9	15	15	16
500–1500 m	-	10	8	8	10	10	8
1500 m to bottom	-	3	5	5	8	8	5
Wind forcing	-	NCEP[b]	ERA-40 and CORE	NCEP and CORE	NCEP	NCEP	QuickSCAT

[a]AG01-R has a horizontal resolution of 0.5° globally and 0.1° in the Madagascar and Agulhas region (20°W-70°E, 47°S-7°S).
[b]In ECCO, data assimilation is conducted on the SSH field and on a collection of vertical temperature profiles.

height-products/global/msla/index.html. We used near-real-time data that were gridded on a 1/3° × 1/3° Mercator grid. The data spanned the period 2003–2008.

2.2. Numerical Models

[11] In this study, we used the output from a total of six OGCM runs. These model runs were chosen because of their spatial and temporal resolutions. Since the dominant frequencies of the transport in the Mozambique Channel are within the range 4/*y*–6/*y* [*Schouten et al.*, 2003; *Harlander et al.*, 2009], we have omitted model outputs with an output resolution of 1/month or lower. Also, we considered only those models that used depth as a vertical coordinate. The considered models are: Estimating the Circulation and Climate of the Ocean (ECCO), the global configuration of the Océan Parallélisé (OPA) model (two runs with different horizontal resolutions and forcing, ORCA025 and AG01-R), Ocean Circulation and Climate Advanced Modeling (OCCAM, two runs with different horizontal resolutions) and the OGCM for the Earth Simulator (OFES). Below, each of these numerical data sets will be briefly described. A summary is given in Table 1. From each data set, the zonal and meridional velocities at the LOCO section across the Mozambique Channel at 16.5°S (see Figure 1) were considered, as well as the SSHA in an area spanning 35°E–55°E and 10°S–25°S.

[12] The ECCO model configuration used is the one that is used for a quasi-operational analysis [*Menemenlis et al.*, 2005]. The model is based on the Massachusetts Institute of Technology general circulation model (MITgcm) [*Marshall et al.*, 1997]. Its output is available on www.ecco.jpl.nasa.gov/, from which we analyzed the data set with Kalman filter assimilation. The output data set started in 1993 and ended in 2008 with a 10 day output interval. It has a zonal grid spacing of 1° and a meridional grid spacing increasing from 1/3° within 10° of the equator to 1° poleward of 22°N/S. There are 37 vertical levels in the Mozambique Channel, with a vertical resolution of 10 m in the top 150 m. The time integration of the run was carried out with a 1 hour time step. It uses a horizontal biharmonic diffusion ($k_0 = -10^{13}$ m^4/s) and vertical Laplacian diffusion ($k_0 = 10^{-4}$ m^2/s^2). The model uses the *K*-profile parameterization (KPP) vertical mixing scheme of *Large et al.* [1994], and isopycnal mixing schemes of *Redi* [1982] and *Gent and McWilliams* [1990]. Atmospheric forcing was applied by 12 hourly wind stress, and daily heat and freshwater fluxes from the National Centers for Environmental Prediction (NCEP) [*Kistler et al.*, 2001]. The model is constraint by satellite observations of the sea surface height variability and a collection of vertical temperature profiles [*Menemenlis et al.*, 2005].

[13] The ORCA025 run [*Madec*, 2006] was performed by the Royal Netherlands Meteorological Institute (KNMI) as part of the DRAKKAR project [*Penduff*, 2005]. The run has a 1/4° horizontal resolution and 32 layers in the Mozambique Channel. This run stretches from 1968 to 2001 with a 5 day mean output. The time step of the model was 1440 s. It has a horizontal biharmonic eddy viscosity (-1.5×10^{11} m^4/s) and a turbulent eddy kinetic-energy-dependent vertical viscosity. The run was forced by a mix of ERA-40 data [*Uppala et al.*, 2005] and Consortium for Oceanic Research and Education (CORE) [*Griffies et al.*, 2008] (the DFS3 data set (L. Brodeau et al., An ERA40 based atmospheric forcing for global ocean circulation models, submitted to Ocean Modelling, 2009)). The bottom topography uses partial steps with a minimum thickness of 25 m.

[14] The AG01-R run was conducted with a nested model [*Biastoch et al.*, 2008a, 2008b]. It consists of a global model at 0.5° horizontal resolution (ORCA05, *Madec* [2006]) and is also part of the DRAKKAR project [*Penduff*, 2005]. In the region 20°W–70°E, 47°S–7°S, a 1/10° model is nested using two-way nesting. The model has 32 vertical layers at the section and uses a bi-Laplacian scheme for the horizontal viscosity ($k_0 = -8.5 \times 10^{11}$ m^4/s for the global model and -2.125×10^{10} m^4/s for the nest), and a vertical Laplacian diffusion of $k_0 = 10^{-4}$ m^2/s, both globally and nested. In the mixed layer, a 1.5 level turbulent kinetic energy closure scheme is used. The run has a 5 day mean output and stretches from 1968 to 2005. The time steps used in the integration are 2160 s for the global model and 540 s for the nest. The atmospheric forcing is applied by NCEP-National Center for Atmospheric Research (NCAR) reanalysis and CORE [*Griffies et al.*, 2008]. The bottom topography uses partial steps with a minimum thickness of 25 m.

[15] The OCCAM model [*Webb et al.*, 1998; *Coward and de Cuevas*, 2005] was derived from the Bryan-Cox-Semtner general ocean circulation model. In this study, we analyzed the output of model runs 103 and 401 (available at www.noc.soton.ac.uk/JRD/OCCAM/EMODS/select.php), spanning

the period from 1989 to 2005. Run 103 has a 1/4° horizontal resolution, while run 401 has a 1/12° resolution. These runs will be referred to as OCCAM025 and OCCAM008, respectively. Both runs have a 5 day mean output (using a baroclinic timestep of 900 s for OCCAM025) and a total of 47 layers in the vertical direction at the section, with 14 layers in the top 100 m. Since the runs were started in 1985 from Levitus temperature and salinity, and zero velocity, and thus, had a shortened spin up (B. A. de Cuevas, personal communication, 2007), the initial years of the output (1989–1992) were not used for the analysis. Therefore, these data sets stretch from January 1993 to December 2004. OCCAM uses Laplacian diffusion (horizontal viscosity is 2×10^2 m^2/s for OCCAM025 and 5×10 m^2/s for OCCAM008, and a vertical mixing coefficient of 10^{-4} m^2/s). In the mixed layer, the KPP vertical mixing scheme is used [*Large et al.*, 1994]. Atmospheric forcing was applied by NCEP 6 hourly forcing [*Coward and de Cuevas*, 2005]. OCCAM uses partial grid cells for the bottom topography.

[16] OFES [*Sasaki et al.*, 2008] is based on the Modular Ocean Model version 3 (MOM3) [*Pacanowski and Griffies*, 1999]. The model has a 1/10° horizontal resolution and a total of 43 vertical layers at the section. The data has a 3 day mean output and stretches from 2000 to 2006. The model run uses a baroclinic time step of 200 s and a barotropic time step of 4 s. The biharmonic horizontal viscosity coefficient is calculated, as in *Smith et al.* [2000], and has a value of -2.7×10^{10} m^4/s. The vertical viscosity is calculated using the KPP [*Large et al.*, 1994]. The run is forced by daily mean values of the NCEP/NCAR reanalysis products and QuikSCAT winds. Partial grid cells are used for the bottom topography.

3. General Characteristics of the Time Series

3.1. Mean, Standard Deviation, and Power Spectra

[17] The time-mean meridional velocities (Figure 2) of the observations consist of three "cores": a strong southward flow at the near surface off the African coast, a weaker northward flow at the near surface off the Madagascar coast, and a weak northward Mozambique undercurrent at the African continental slope [*de Ruijter et al.*, 2002]. The two "cores" near the surface are a result of the southward propagating Mozambique Channel eddies [*Ridderinkhof and de Ruijter*, 2003; *Harlander et al.*, 2009]. A similar flow structure is observed in most numerical models (AG01-R, OCCAM025, OCCAM008, and OFES), although their flow is too strongly surface-intensified. These four numerical model runs simulate Mozambique eddies at the measurement section (the structure of the eddies will be discussed in section 4). No eddies are simulated in ECCO and ORCA025. These models simulate two "cores": the strong, southward near-surface flow at the African coast and a weak northward undercurrent. In ORCA025, eddies are observed further downstream, south of 20°S, while the horizontal resolution of ECCO does not suffice to simulate eddies.

[18] Time series of the volume transport and their power spectra are shown in Figures 3 and 4. The power spectra are compared to an autoregressive(1) [AR(1)] red noise spectrum, which was computed with a Monte Carlo simulation with 5000 members. The seasonal cycle is not taken into account in the calculation of the red noise spectrum because it is a deterministic signal, i.e., it is driven by external forcing. The AR(1) spectrum was therefore based on each time series subtracted by a sine function with a period of 1 year, which was fitted to the time series. The model spectra have been interpolated to the frequency bins of the observed spectrum.

[19] The mean of the southward transport over the full time series in the observations is 16.7 Sv. Two models (ECCO and ORCA025) estimate a higher transport, while others (OCCAM025 and OFES) estimate a lower transport (for an overview, see Figure 5). Note, however, that the time series of LOCO is relatively short and that large variations on the interannual time scale have been observed [*Ridderinkhof et al.*, 2010]. The mean transport in the models is not solely dependent on grid size; of the two models with a horizontal resolution of 1/4° (ORCA025 and OCCAM025), one overestimates the transport and the other one underestimates it (23.6 and 11.3 Sv, respectively).

[20] Stricking is the difference in transport variability. The transport in the observations ranges from 65 Sv southward to 45 Sv northward (Figure 3). The extremes in the model runs are much smaller. The standard deviation of the observations (13.5 Sv, calculated as the square root of the integrated variance within the frequency band of 0–18/y) is about twice as large as that of the model runs (Figure 5). This difference in transport variability is also clear in the power spectra (Figure 4), Especially at frequencies higher than 1/*y*, the variability of the observations is much larger than that of all model runs.

[21] Two frequency ranges in the observations have a spectral density that is clearly distinguishable from the red noise spectrum. The first is a peak around 5.5/*y*–6/*y*, which is associated with Rossby waves and the Mozambique Channel eddies [*Schouten et al.*, 2003; *Harlander et al.*, 2009]. The other range has a lower spectral density and ranges from 7/*y* to 9/*y*. This range is most presumably associated with barotropic instability in the strongly sheared flow near Cape Amber, the northern tip of Madagascar [*Quadfasel and Swallow*, 1986; *Schott et al.*, 1988; *Biastoch and Krauss*, 1999; *Schouten et al.*, 2003].

[22] The spectral density of the model runs is not significant with respect to the red noise spectrum in the 7/*y*–9/*y* frequency range, and only AG01-R and OFES simulate a narrowly significant variability in the 5/*y*–6/*y* frequency range. Nonetheless, even for AG01-R and OFES, the spectral density in this frequency range is very small compared to the observations.

[23] The transport variability benefits somewhat from an investment in the horizontal resolution. Although all models underestimate the variability of the transport, the power spectra of the models with a higher horizontal resolution are slightly closer to that of the observations than that of models with a coarser resolution.

3.2. Seasonal Cycle

[24] The frequency with the highest spectral density in all of the numerical model runs is 1/*y*, the seasonal cycle (Figure 4). In all numerical models, this signal is higher than the AR(1) spectrum, which was discussed in the previous section. This is in contrast to the observations, where the seasonal cycle is lower than the AR(1) spectrum,

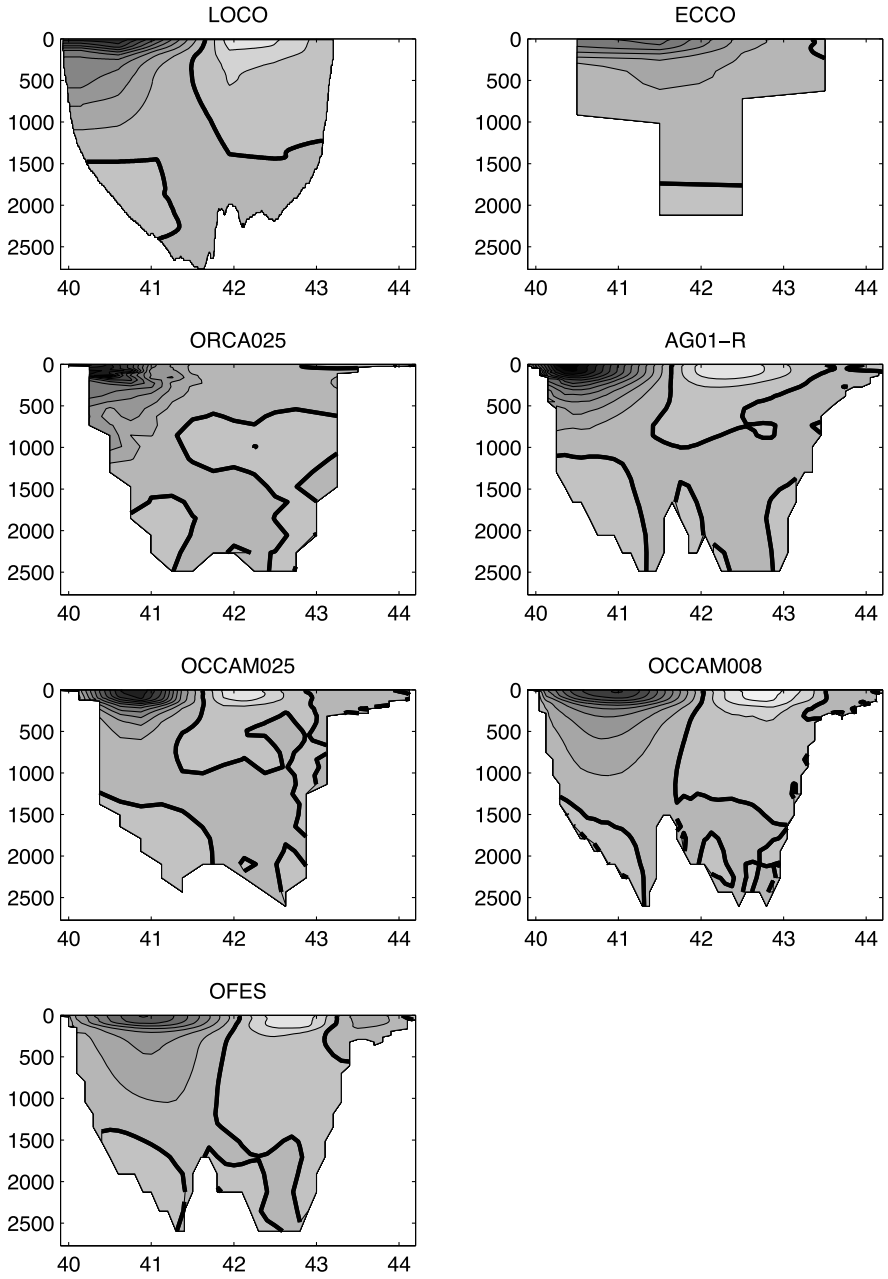

Figure 2. Time-averaged meridional flow for the observations (LOCO) and the six numerical model runs. Contours are drawn every 5 cm/s, the lighter (darker) colors denote northward (southward) flow, and the thick contour denotes the zero line. All data sets have a strong southward flow in the upper west of the section and a northward/weak flow in the upper east. A northward flowing undercurrent is observed in all data sets.

and is of the same size as the variability at low frequencies ($0.5/y$) and in the $5.5/y$–$6/y$ range. The main reason for this difference is the underrepresentation of the variability at higher frequencies ($f > 1/y$) in the models, which decreases the spectral density of the red noise spectrum at the lower frequencies. This difference is clearly visible in the transport time series (Figure 3). No clear seasonal cycle exists in the observations, whereas in each numerical model run, a seasonal cycle can be detected by eye in the time series.

[25] To extract the seasonal cycle from each data record, a sine with a period of one year was fitted to each time series. This method does not discriminate between cycles that are significant (in the models) or insignificant (in the observations). The amplitudes of all the seasonal cycles (Figures 5 and 6) range between 4.1 Sv (ECCO) and 8.3 Sv (AG01-R). The amplitude of the seasonal cycle in the observations is 5.0 Sv, comparable to those of most numerical models runs. The phases of the cycle in all data sets but ECCO are also similar, with the maximum southward transport in September and the minimum in March. The phase of ECCO is belated by a month (Figure 6).

[26] The seasonal cycle is primarily related to the wind stress pattern in the Indian Ocean. *Matano et al.* [2002, 2008] showed that regional barotropic processes control the

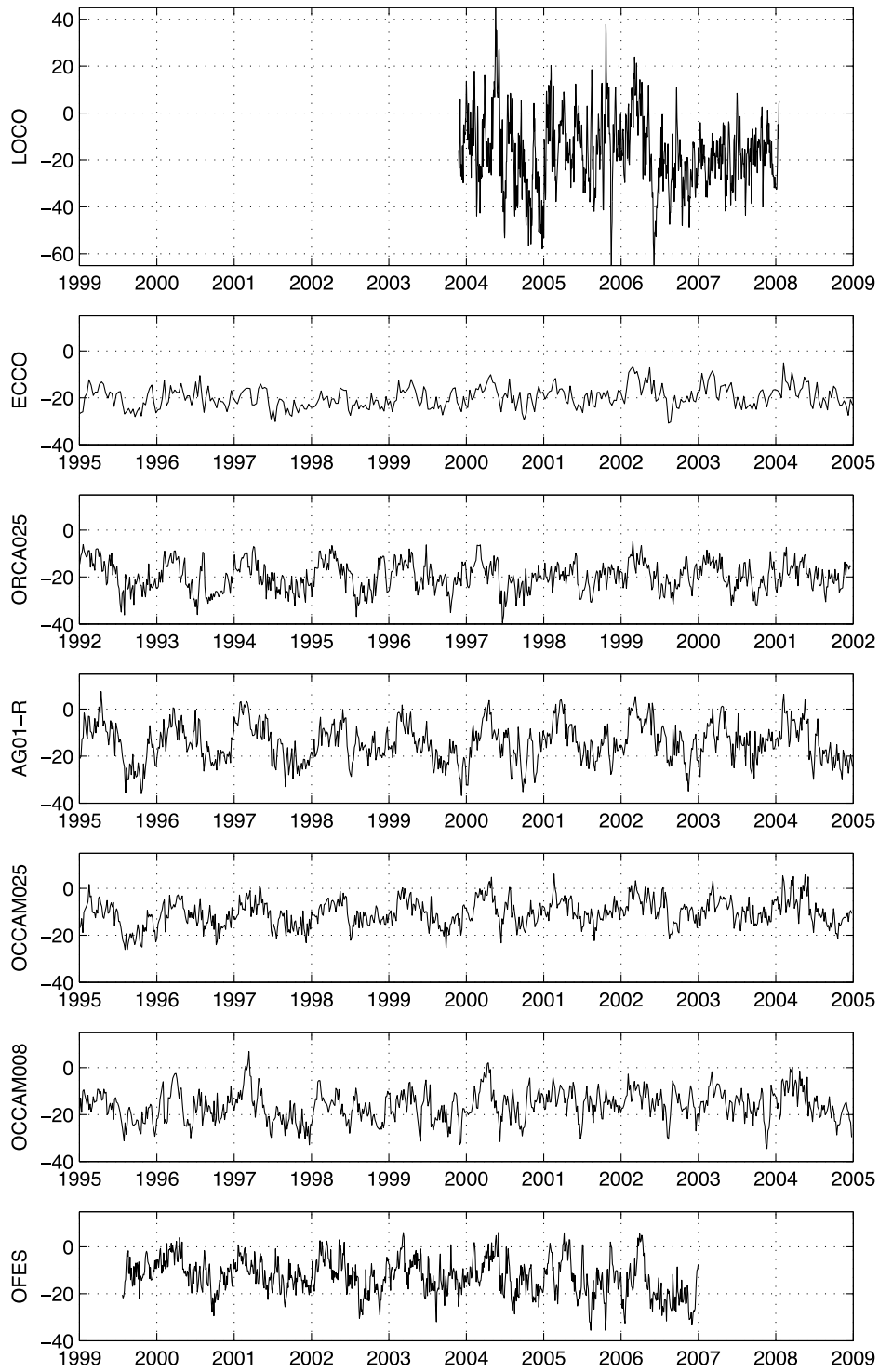

Figure 3. Transport time series (Sv) for the observations (LOCO) and the six model runs in the Mozambique Channel at 16.5°S. Negative values denote southward transport. For the runs ECCO, ORCA025, AG01-R, OCCAM025, and OCCAM008, a 10 years selection of the data has been made. In the numerical model time series, a seasonal cycle is observed by eye, while no clear seasonal cycle exists in the LOCO time series.

seasonal variability in the South Indian Ocean. The origin of the seasonal variability of the transport in the Mozambique Channel should therefore be found west of 75°E (see *Matano et al.* [2008], Figure 3a), since the barotropic seasonal variability cannot cross the Mid-Indian Ridge. Applying the linear island rule [*Godfrey*, 1989] on the wind stress, west of 75°E, gives a seasonal cycle in the Mozambique Channel transport of 4.5 Sv. The lag between the wind forcing and the transport is about a month, consistent with the propagation speed of the seasonal cycle [*Matano et al.*, 2008].

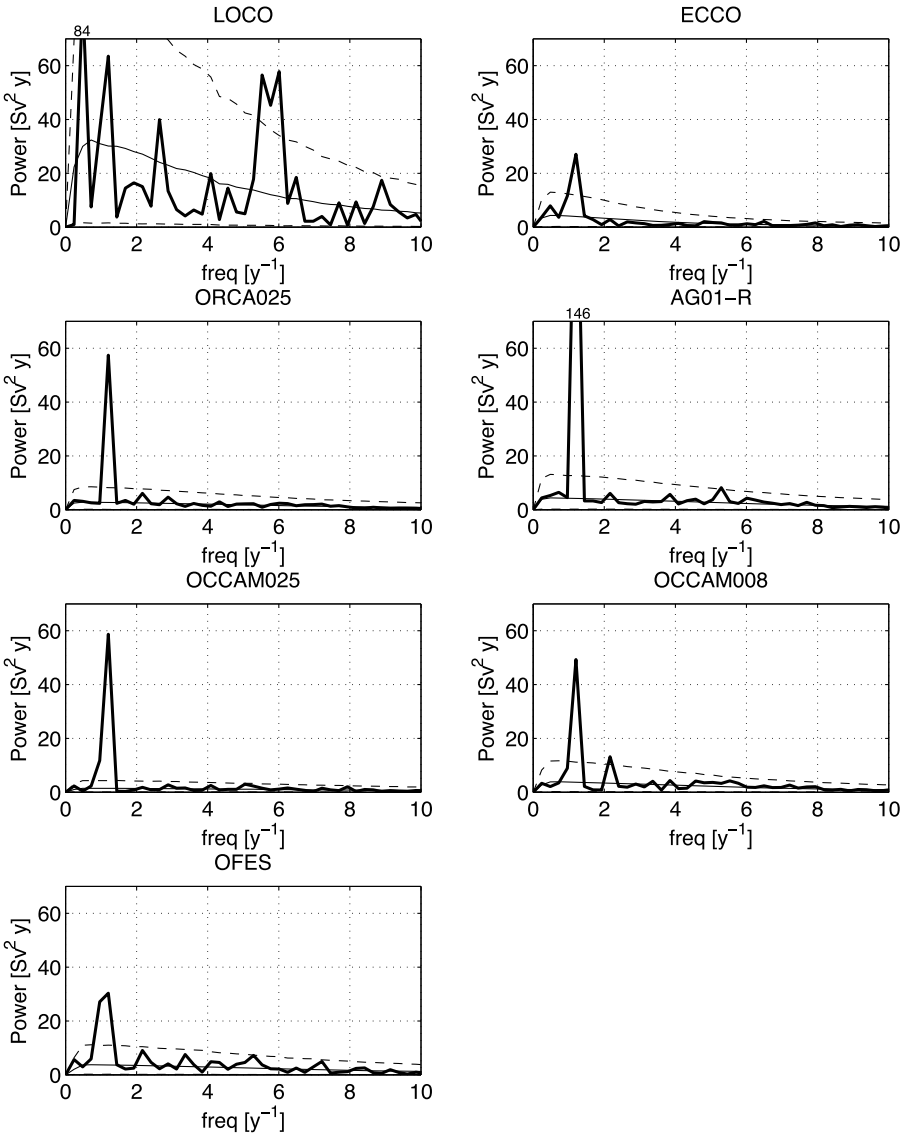

Figure 4. Power spectra of the transport time series (thick lines) for the observations (LOCO) and the six model runs in the Mozambique Channel at 16.5°S. The thin lines denote the mean of an AR(1) spectrum (solid line), and the 95% and 5% confidence intervals (dashed lines). The spectra of the models were interpolated to fit the frequency axis of the observations. The power at the $1/y$ frequency is quite similar for all time series. On the other hand, the power at high frequencies in the models is clearly underrepresented.

[27] In conclusion, there is, indeed, a seasonal cycle in the observations, explained by varying upstream wind forcing. A similar seasonal cycle is simulated in the numerical model runs. However, the seasonal cycle in the models is dominant because it is the only frequency that is well resolved. The spectral density at all other frequencies is underrepresented. In contrast, the seasonal cycle in the observations is not dominant, since it is overshadowed by the variability at other frequencies. Hence, the origin of the discrepancy should be sought in the underrepresentation by the models of variability at frequencies other than $1/y$.

3.3. Structure With Depth

[28] To better understand the difference between the models and the observations at frequencies higher than 1/y, we have repeated the above analysis for the transport at several depth ranges. For example, if the difference between observation and model transport variability would be largest near the surface, then the variability in atmospheric forcing could be insufficient. However, if the difference would be largest in the bottom layers, then the interaction with the bottom topography could be wrongly modelled.

[29] Our results appeared clearest by dividing them into two depth ranges: the transport shallower than 1500 m, and that between 1500 m and the bottom. Figure 7 shows the standard deviation of the band-pass-filtered transport of frequencies between $1/y$ and $10/y$, for the two depth ranges. In this frequency band, both the frequency band $5/y$–$6/y$ and $7/y$–$9/y$ are represented. Remarkably, the three high-resolution model runs (AG01-R, OCCAM008, and OFES)

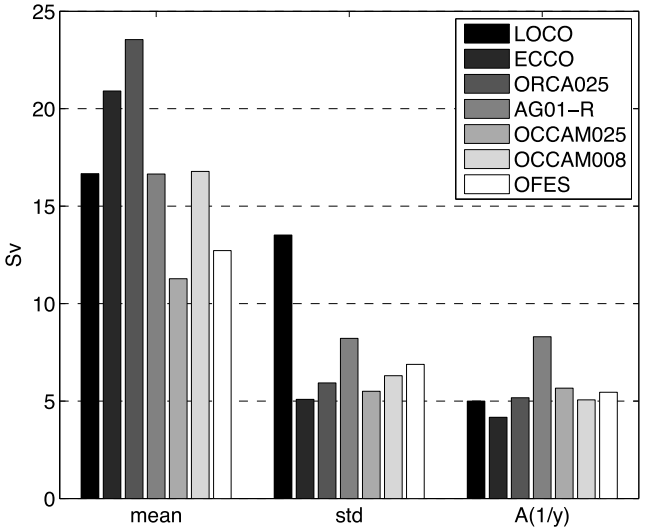

Figure 5. Mean of the southward volume transport at 16.5°S, its standard deviation (std), and the amplitude of the 1/*y* frequency (A(1/*y*)) in the observations (LOCO) and the six model runs. The standard deviations have been calculated as the square root of the the integrated variance between frequencies of 0−18/*y*.

have about the same standard deviation in the transport deeper than 1500 m, as is observed in the observations (1.9−2.6 Sv). However, for the depth range above 1500 m depth, the numerical model runs fail to simulate about half of the variability of the observations (4.4−4.9 Sv for the three high-resolution models versus 9.1 Sv for the observations). As expected, the high-resolution models perform better than the low-resolution models.

[30] The largest differences between observations and numerical models were observed between 500 and 1500 m depth (not shown). At this depth, the variability is mainly related to baroclinic Rossby waves and the Mozambique Channel eddies (5/*y*−6/*y*), and most presumably to barotropic instability (7/*y*−9/*y*). Near the surface, the variability is forced by both internal processes and local atmospheric forcing. Variability because of the local atmospheric forcing is quite well resolved by the numerical models, which makes the relative difference between variability in the observations and the models near the surface smaller.

4. FOCUS on the 5/*y*−6/*y* Frequency Range: Eddies and Rossby Waves

[31] As pointed out above, the most important variability in the observations is concentrated in the frequency range 5/*y*−6/*y* (Figure 4), while the spectral density in this frequency range is not particularly well represented by the OGCMs. Moreover, the largest difference between the observations and the models is in the upper layer variability, above 1500 m. In this section, we will therefore focus on the typical features that are observed in this frequency range and depth scale: Mozambique Channel eddies and Rossby waves [*Schouten et al.*, 2003; *Harlander et al.*, 2009].

[32] *Harlander et al.* [2009] studied a series of snapshots of the meridional velocity of an eddy at the LOCO mooring section. As the eddy moves southward, the pattern at the section has a westward phase propagation, suggesting a southwestward direction of the eddy. Then, when the eddy has nearly passed through the section, a southward current is observed at the eastern side of the section, which is moving westward as well. After the analysis by empirical orthogonal functions (EOFs) and principal oscillation pattern (POP) analysis, *Harlander et al.* [2009] concluded that this pattern was caused by the superposition of Mozambique Channel eddies and westward propagating Rossby waves. In the following, we use the analysis methods of *Harlander et al.* [2009] to compare the data of the observations with that of the numerical models. Only those numerical models

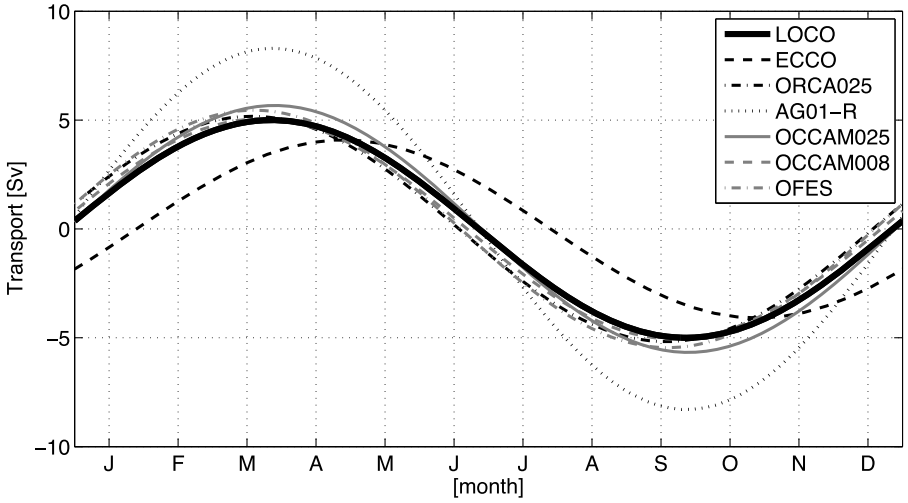

Figure 6. Seasonal cycle of the transport in the observations (LOCO) and the six model runs. The seasonal cycle was obtained by fitting a sine function to the transport time series with a period of one year. The seasonal cycle is quite similar for all data sets. It has a higher amplitude in AG01-R and a phase shift of about one month in ECCO.

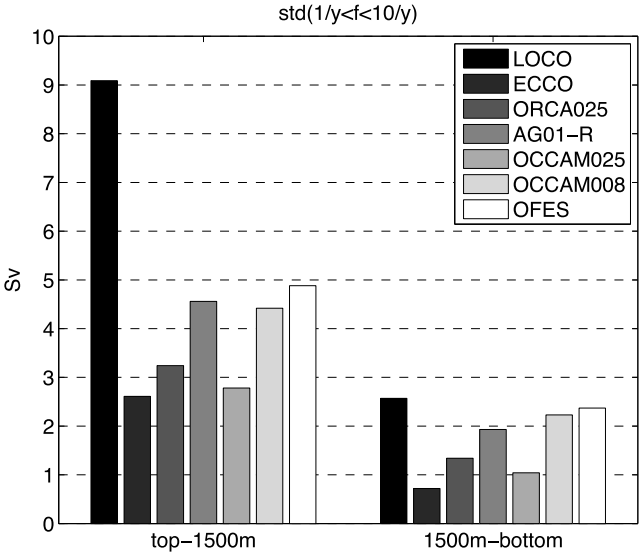

Figure 7. Standard deviation of the transport time series, band filtered between the frequencies of 1/*y* and 10/*y*, for the transports (left) shallower and (right) deeper than 1500 m for the observations (LOCO) and the six model runs. The variability at depths shallower than 1500 m is underrepresented in the numerical models.

with eddies around 16.5°S (AG01-R, OCCAM025, OCCAM008, and OFES) will be studied.

[33] Figure 8 shows the first two EOFs of each of the five data sets. These EOFs were calculated from the meridional velocities from which the seasonal cycle was removed. The time series of these ten EOFs have their main variability in the frequency band 5/*y*–6/*y*.

[34] As shown by *Harlander et al.* [2009], the first two EOFs of the observations were identified as the superposition of Mozambique Channel eddies and a westward-propagating Rossby wave. EOF2 looks like EOF1, but is phase shifted by $\pi/2$, indicating westward propagation. The main part of EOF1 is explained by *Harlander et al.* [2009] by a southward-propagating anticyclonic eddy, while the remaining part of EOF1 together with the main part of EOF2 was explained as a westward-propagating Rossby wave.

[35] The four numerical models show a similar structure of the first two EOFs, although the ratio between the explained variances of EOF1 and EOF2 in the models is slightly lower than in the observations. In OCCAM008, the variance explained by the two EOFs is almost equal. This can partly be explained by the different orientation of the "mooring sections" in the observations and the models (Figure 10). The section of LOCO is tilted slightly in a southeastward direction, the sections in the models are zonally orientated. From altimetry, it is observed that the eddies pass the section in a southwestward direction. Therefore, their propagation in the models has a small parallel (westward) component to the section. Although one cannot determine it directly from these EOFs, which are based on meridional velocities, this extrawestward motion is probably captured by EOF2.

[36] The EOF structures of the observations reach depths of 1500 m. The structures in OFES are similarly deep, while the structures in OCCAM025 are very shallow and reach depths of only 280 m. To examine the vertical structure in more detail, a velocity-depth plot has been made of EOF1 (Figure 9): for each depth, the mean velocity of EOF1 and the maximum absolute anomaly relative to that mean were determined. If EOF1 can be considered as a pure eddy, this maximum absolute velocity anomaly represents the tangential velocity of an eddy. As mentioned above, this assumption is not completely true, as EOF1 is regarded as the superposition of an eddy with a westward-propagating Rossby wave. The tangential velocity is therefore an estimation for all data sets. We did, however, obtain qualitatively similar results with individual eddies, and the EOF analysis gives us an estimate over all eddies in the time series.

[37] The thus-obtained eddy structure in the observations consists of two parts: above 380 m depth, the tangential eddy velocity strongly decreases with depth, while deeper than 380 m, the decrease in tangential velocity is much less. The eddies in the observations have a strong barotropic component (also shown in *de Ruijter et al.* [2002]). Near the surface, the tangential velocities of the eddies in the OGCMs range around the observations: OCCAM008 and OFES are a bit too strong, while AG01-R and OCCAM025 are a bit too weak. Also at depth, the tangential velocities of the eddies in the models range around the LOCO values. The eddies of the three high-resolution models (AG01-R, OCCAM008, and OFES), in particular, have tangential velocities at depth that are comparable to that of the observed eddies. This is a major improvement from the former generation models with a lower horizontal resolution, such as OCCAM025, which have eddies that are too much surface intensified and very weak at depth [*Schouten et al.*, 2003]. We, thus, find that the eddy structure in the models cannot be the cause of the underrepresentation of the variability in the frequency range 5/*y*–6/*y*. Related to this, it should be noted that the contribution of a passing eddy to the transport variability is very small. A "perfect" eddy with a zero translational velocity does not contribute to the total transport; a result that is independent of the tangential velocity. When an eddy is propagating, only the sea level anomaly related to the eddy contributes to the transport variability. An eddy with a sea level anomaly of 30 cm and a propagation speed of 6 km/day [*Schouten et al.*, 2003] contributes an extra 3 mSv to the transport, which can be neglected relative to the total transport variability.

[38] In contrast to the eddy structure, a major difference in the formation area and formation mechanism of the eddies was found between the observations and the models. For the four models and in the observations, four years of eddy paths have been tracked by manually following the positive sea surface height (SSH) anomalies through the Mozambique Channel (Figure 10). The criteria used for the identification of an eddy were that the eddy should have at least an SSH anomaly of 20 cm and should be relatively circular (ratio of meridional and zonal diameter of less than 3). Only eddies that crossed the section at 16.5°S were taken into account. In addition to the eddy paths, Hovmuller plots of the surface velocities at the mooring section were analyzed (Figures 11 and 12).

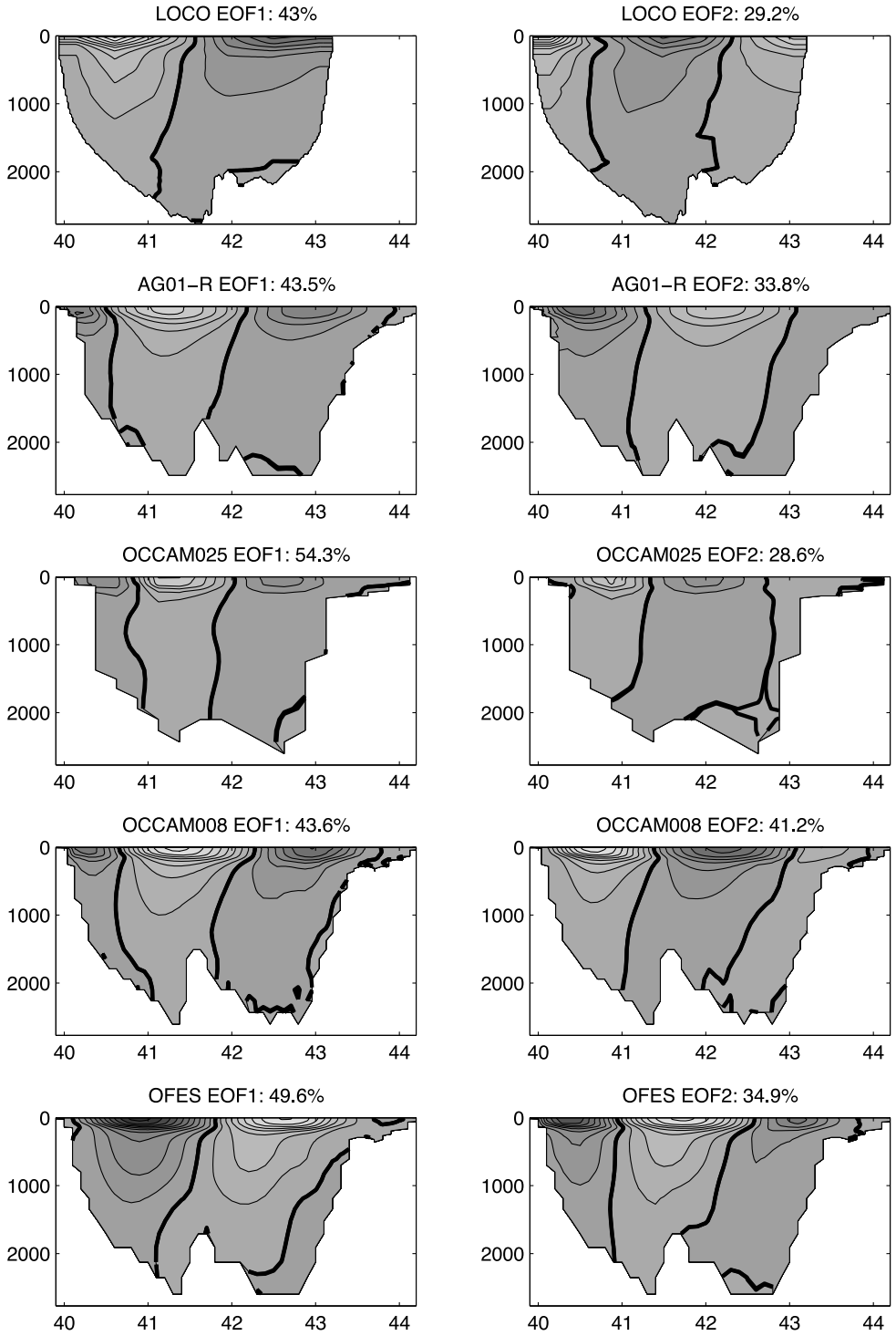

Figure 8. (left) Empirical orthogonal function 1 (EOF1) and (right) EOF2 for the meridional velocities, of which the seasonal cycle was removed, of the observations (LOCO) and the four numerical model runs that simulate eddies at the mooring section. Contours are drawn every 5 cm/s, and the thick contour denotes the zero line. The amount of variance explained by each EOF is stated.

[39] In the observations, most eddies that pass the mooring section are formed relatively close to the mooring section (Figure 10, AVISO). Some eddies are formed further north, near Cape Amber at the northern tip of Madagascar, but these eddies dissolve north of the mooring section, and are therefore not shown. The mechanism of the formation of eddies in the observations was proposed by *Ridderinkhof and de Ruijter* [2003] and verified by *Harlander et al.* [2009] (also see Figure 11, 12 LOCO): first, a strong southward flow along the Madagascar coast exists, e.g., at

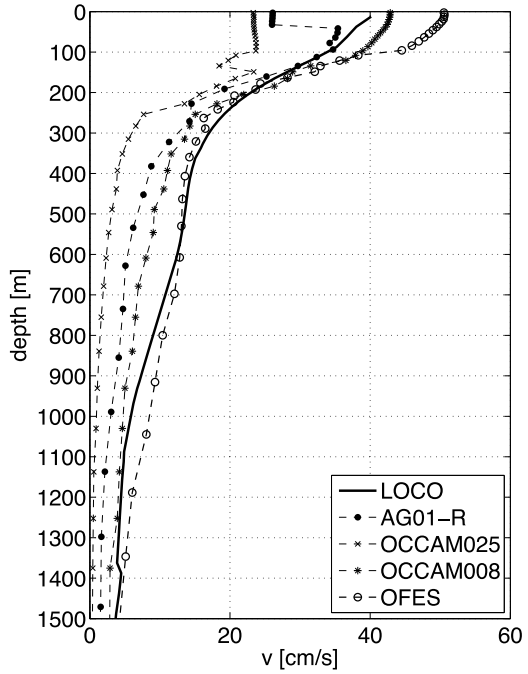

Figure 9. Tangential velocity of eddies in the observations (LOCO, solid line) and the four numerical models with eddies (dashed lines with markers), obtained via EOF analysis (see text for details). The markers indicate the depth levels of the models. The higher resolution models (AG01-R, OCCAM008, and OFES) represent eddies well.

days 80 and 150. This current is a western boundary current flowing along the Northern Mozambican coast, which overshoots at the narrows. The maximum of the southward flow propagates westward, presumably by the interaction with a Rossby wave. Then, a strong anticyclonic eddy develops (days 120 and 170). Also, the eddy itself has a small westward propagation (compare the position of the maximal westward flow at days 120 and 140).

[40] The surface flow in the observations is thus characterized by two main structures that alternate: the strong southward current and the eddy formation. Also, at the first eddy event in the 200 days LOCO time series, the eddy is preceded by a southward current, although this current flows at the western side of the Mozambique Channel (day 30 of Figure 12, LOCO).The alternation between current and eddy, which has a frequency of $5.5/y$, results in variability of the transport at the same frequency.

[41] The eddies in the three high-resolution model runs (AG01-R, OCCAM008, and OFES) are mainly formed further north in the channel (Figure 10). They propagate with the background flow through the mooring section. Altimetry data suggest that the Rossby waves in these models do not play the same role as in the observations. Instead of facilitating the formation of an eddy, they seem to strengthen the eddy that has already been formed north. They also give the eddies a westward impulse and bend their path from southward to southwestward. In the lower resolution model OCCAM025, the eddies are formed at the mooring section, like in the observations, but without the interaction with a Rossby wave (Figures 11, 12-OCCAM025). Moreover, instead of occupying the whole section, they are small disturbances in the background flow.

[42] In all four numerical model runs, there is no alternation at the mooring section between currents and eddies (Figures 11 and 12). For AG01-R and OCCAM025, eddies are seen at days 30, 120, and 180 (AG01-R), and days 0, 70, and 120 (OCCAM025). These eddies are only small disturbances in the background flow, which is a southward current at the western side of the Mozambique Channel. As the effective transport of an eddy moving in a background flow is close to the transport of the background flow, the resulting transport time series does not have strong variations in the eddy frequency range ($5/y$–$6/y$). In OCCAM008 and OFES, only eddies pass the mooring section, as can be clearly seen in Figure 12. The eddies in OFES seem to be moving slowly through the section, as in the other data sets, but this does not influence the transport variability. Around day 110 in the OFES data, a southward current is seen east of the previous eddy. However, the zonal mean velocity is very steady, around 5 cm/s, because at the same time, a northward current flows west of the southward current. Again, there is no alternation between southward currents and eddies, which results in a quite continuous transport as well.

5. Discussion

[43] The power spectrum of the Mozambique Channel transport in numerical models could be greatly improved when the formation mechanism and formation location of the eddies is corrected. Why the eddies in the OGCMs passing the mooring section are formed at the wrong location is not precisely understood at this moment. Both in the observations and high-resolution models, eddies are formed near Cape Amber. However, in the observations, these eddies decay and new eddies are formed at the mooring section, while in the numerical models, they propagate through the mooring section. This difference in behavior could be caused by the representation of the bottom topography, with which the eddies interact. For example, the path of the eddies is through the Comores. This island group is not well represented by the OGCMs. In reality, it consists of four major islands (diameter larger than 5 km). OCCAM008 and AG01-R only have one island representing the Comores. In OFES, all four islands can be identified, but they consist of only a few grid points. Deeper down, the AG01-R does better, but OCCAM008 almost closes the gaps between the three westernmost islands, while the gap in reality is about a quarter degree (which would be a distance of three instead of one grid cell for OCCAM008). Nevertheless, the bathymetry close to the Comores is very steep, and the interaction of eddies with this island group might, therefore, not be correctly simulated by the OGCMs.

[44] It is not clear to what extent the location of the LOCO mooring section influences the power spectrum of the transport. As pointed out above, the strong signal at $5/y$–$6/y$ in the observations is mainly because of the formation of eddies close to the section, and therefore, the alternation between southward currents and eddies. Further south, this alternation may not be present, as the eddies propagate in and with the background flow. However, there

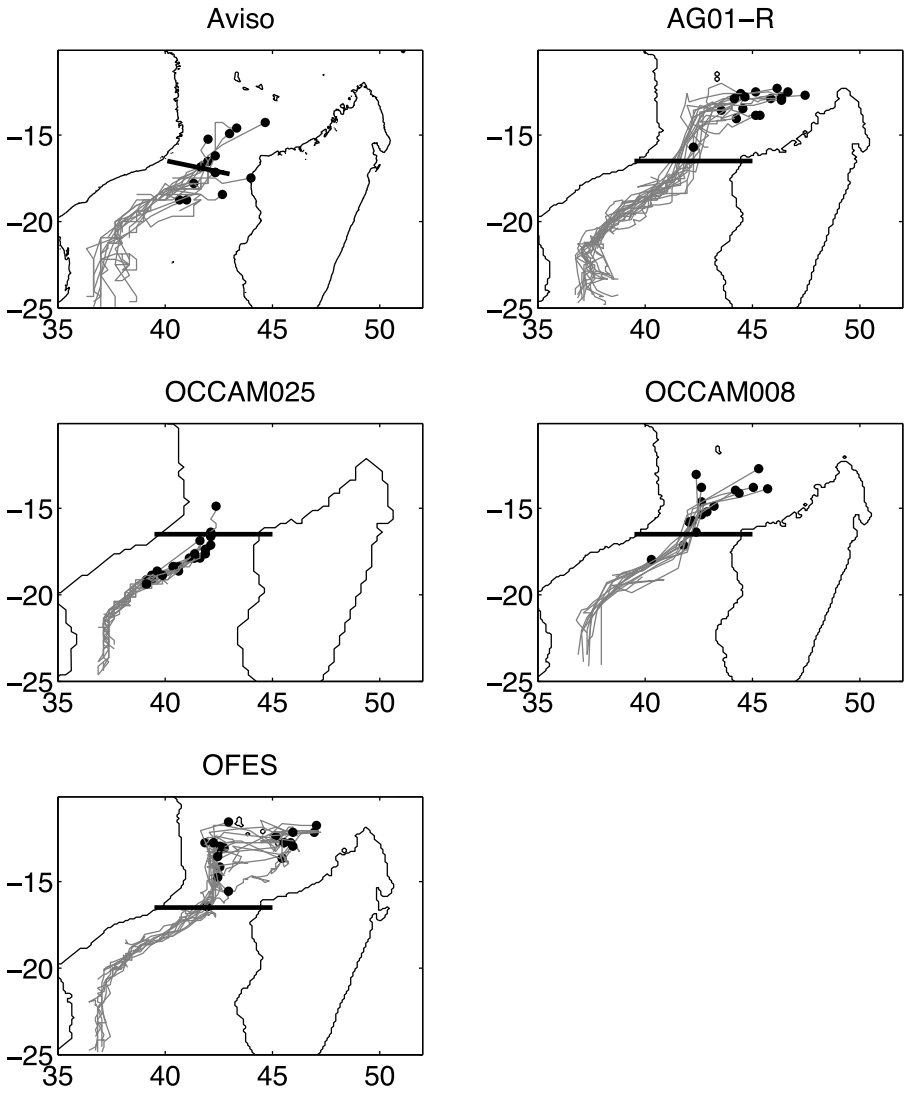

Figure 10. Tracked eddies that pass the mooring section in four years of data for the observations (Archiving, Validation, and Interpretation of Satellite Oceanographic (AVISO) data 2004–2007) and the four models with eddies (2001–2004). The black dot denotes the start of each eddy, and the gray line denotes the eddy path. The black line denotes the measurement section.

are no transport observations to measure the strength of the $5/y-6/y$ signal south of the eddy formation area.

[45] In a sensitivity study to the mooring section location in the numerical models, two extra transport time series at different latitudes (14°S and 20°S) have been extracted from the OCCAM008 data. The power spectra of these two transport time series were not significantly different from the model spectrum at 16.5°S. The formation of eddies in the numerical models north of the mooring section is different from the formation of eddies in the observations. Therefore, we might expect that the power spectrum of the transport near the formation area of eddies in the numerical models will be different from that of the observations.

[46] Apart from the six model runs described above, the analysis was also carried out with data from a 4-year run with the Parallel Ocean Program (POP) model (1/10° horizontal resolution and daily output) [*Dukowicz and Smith*, 1994; *Maltrud and McClean*, 2005]. This run was forced by monthly climatological atmospheric forcing, which includes only a part of the atmospheric forcing variability of the other OGCMs. Therefore, it was not taken into account in the full analysis. Nevertheless, similar results were obtained. The mean southward transport through the Mozambique Channel in POP is 14.6 Sv with a standard deviation of 5.2 Sv. Its seasonal cycle has an amplitude of 5.4 Sv, which is of the same size as the standard deviation. As in the other numerical models, the seasonal cycle exceeds the AR(1) spectrum, while the variability at frequencies higher than $1/y$ is underrepresented. The conclusions drawn in this paper are thus independent of the atmospheric forcing.

[47] The second main frequency range of which the spectral density in the transport of the observations is significant is the range $7/y-9/y$ (Figure 4). Spectral density in this range can be associated with barotropic instability at Cape Amber [*Quadfasel and Swallow*, 1986; *Schott et al.*,

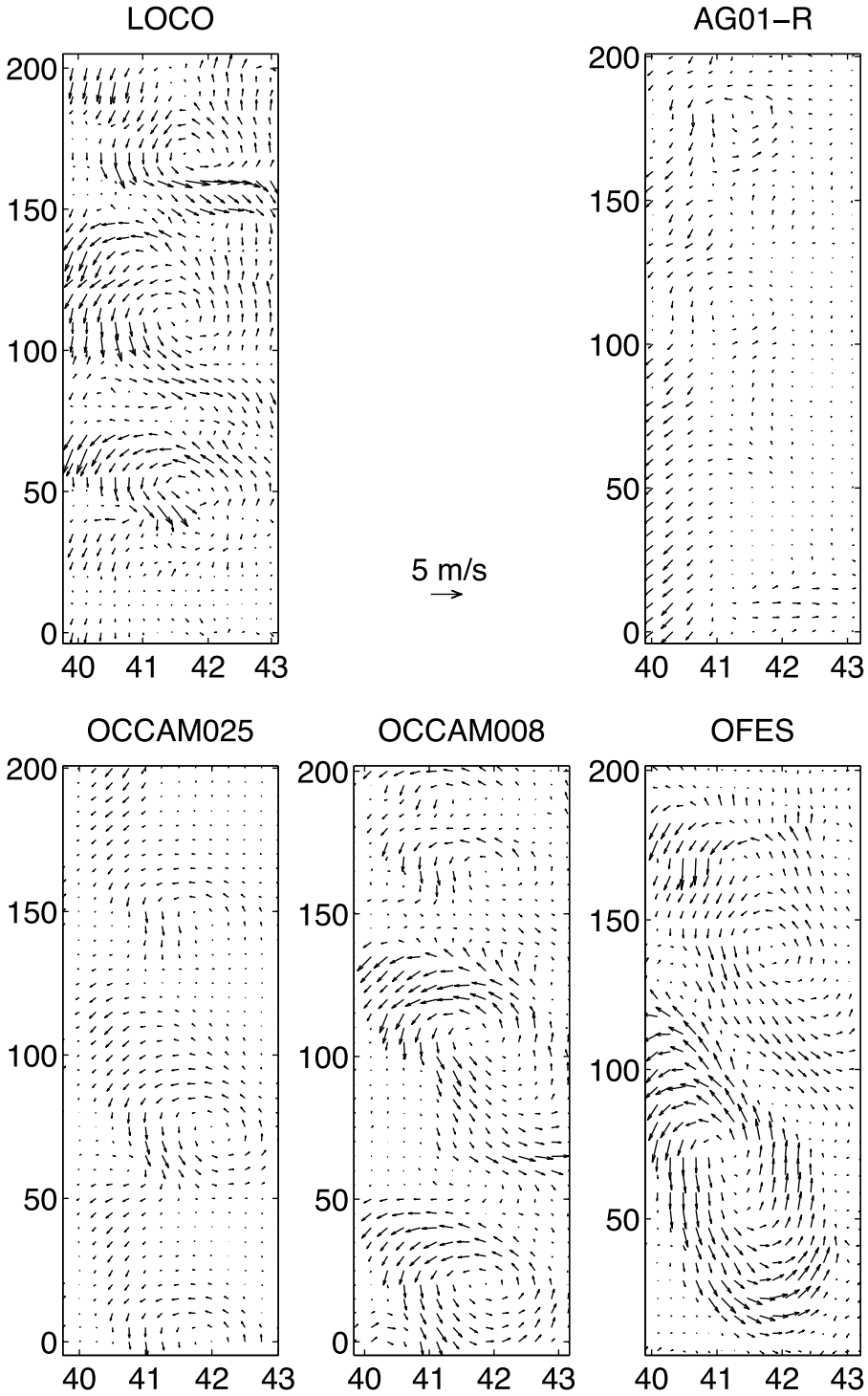

Figure 11. Hovmuller plots over 200 days of the near-surface velocity at the section for each data set containing eddies. Vectors show speed and direction. The first day of the plots is July 18, 2004 (LOCO), December 24, 2001 (AG01-R), January 9, 2001 (OCCAM025 and OCCAM008), and March 16, 2001 (OFES). A correspondence between space and time exists under the assumption that the eddy moves by a constant speed while preserving its structure. A more elaborate discussion on these kind of plots can be found in *Harlander et al.* [2009].

1988; *Biastoch and Krauss*, 1999; *Schouten et al.*, 2003]. The shear leading to this instability is very strong. The along-coast velocity increases from zero at the coast to 1 m/s at 30 km offshore [*Swallow et al.*, 1988]. Such a narrow boundary layer may not be fully resolved by numerical models with a 1/10° resolution. It has been shown that models do solve the barotropic instability [e.g., *Biastoch and Krauss*, 1999], but they might not resolve all the energy

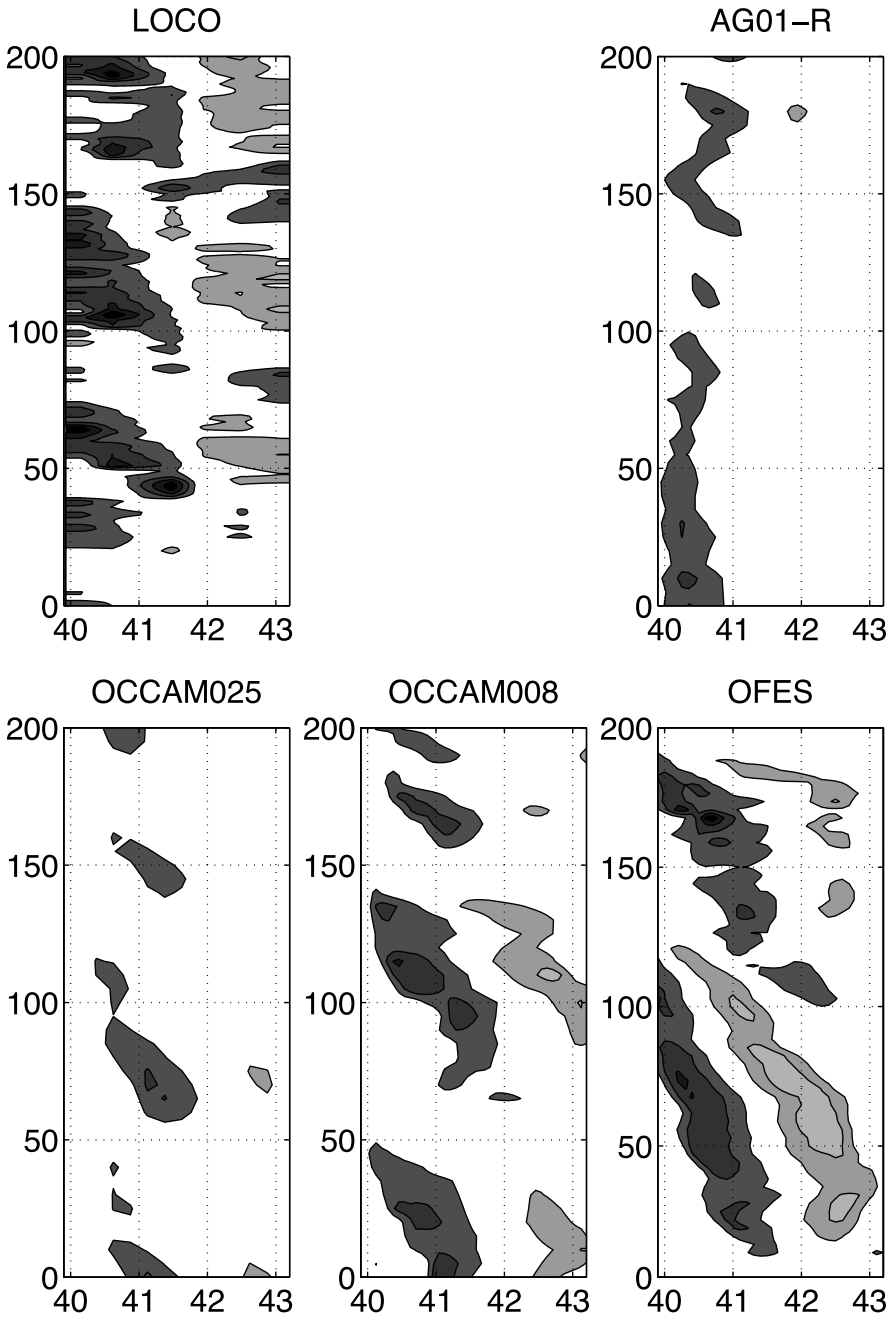

Figure 12. Same as Figure 11, but for meridional velocity only. Contours are plotted every 50 cm/s, the zero line is omitted and darker (brighter) colors denote southward (northward) flow. The Hovmuller plot of the observations clearly shows an alternation between southward currents and eddies; such an alternation does not exist in the models.

at this frequency that is observed in the observations. This might explain why the spectral density in this range in the numerical models is less than in the observations.

6. Conclusions

[48] In this study, we analyzed the temporal variability of the observed transport through the Mozambique Channel and compared it to transports simulated by six OGCMs. An important difference between the observations and the numerical models regards the dominance of the seasonal cycle. This signal is relatively weak in the observed transport, while it is dominant in the numerical model transport. However, the seasonal cycles of the observations and numerical models are similar in strength and phase. The cycle can be explained by the yearly variation of the wind forcing in the Indian Ocean west of 75°E. Thus, a seasonal cycle in the Mozambique Channel transport does exists, and has an amplitude of 5 Sv.

[49] The seasonal cycle in the models is dominant because the spectral density at other frequencies is not well

represented. Main deviations from the observations were found at depths shallower than 1500 m and in the $5/y-6/y$ frequency range.

[50] The three high-resolution models (AG01-R, OCCAM008, and OFES) simulate the Mozambique Channel eddy structure quite well; the barotropic component of the eddies in these models was stronger and closer to eddies in observations than in the lower resolution model OCCAM025 and previous studies [*Schouten et al.*, 2003]. However, in all models, the formation mechanism of the eddies was found to be different from that in observations. Research by *Ridderinkhof and de Ruijter* [2003] and *Harlander et al.* [2009] suggests that eddies in the observations are frequently formed from an overshooting current near the mooring section in combination with a Rossby wave. This causes an alternation of events at the mooring section, varying between a strong southward current, and the formation and passing of an eddy. This alternation results in a variation of transport in the frequency range of $5/y-6/y$. In the models, on the other hand, the eddies are formed further upstream, and they propagate symmetrically through the section. Altimetry data suggest that the Rossby waves in the models strengthen the eddies that have already been formed and do not play a role in their formation. No alternation similar to the observations was found, which results in a more constant transport in the models.

[51] Our results have implications for the use of numerical model output in the Southwest Indian Ocean. The time-mean dynamics of the system seems to be well resolved by the numerical models and also by the eddy structure in the high-resolution models. Studies with numerical models that use only these characteristics should therefore not encounter problems. For example, *Biastoch et al.* [2008b] did a sensitivity experiment to whether Mozambique Channel eddies influence the interocean exchange in the Agulhas system. In that study, it was not relevant where the Mozambique Channel eddies were formed, but their strength should be close to observations, as should the amount of Mozambique Channel eddies per year.

[52] On the other hand, the wrongly estimated formation area of the eddies could have implications for the water masses that are trapped by the eddies. Also, studies involving local biology or sediment transport should be careful in applying these numerical models.

[53] **Acknowledgments.** We thank Jenny Ullgren (NIOZ, Texel) and Uwe Harlander (NIOZ, Texel, currently at BTU-Cottbus, Cottbus) for helping deriving the transport time series for the observations (LOCO). Also, this work would not have been possible without the help and cooperation of a large number of people who willingly shared their model output. Tony Lee, Dimitris Menemenlis, and Hong Zhang (NASA Jet Propulsion Laboratory, Pasadena) suggested to us the ECCO output and made the data available. Camiel Severijns (KNMI, de Bilt) provided the ORCA025 output. Arne Biastoch (IFM-GEOMAR, Kiel) shared the data of AG01-R, and gave us some useful comments. Andrew Coward (NOC, Southampton) provided the OCCAM output on 1/12° resolution. The 1/4° resolution run was made freely available on the Web by the NOC. The OFES data were made available by Yukio Masumoto (University of Tokyo, Tokyo and JAMSTEC, Yokosuka). Mathew Maltrud (LANL, Los Alamos) made the POP data available. The crew, technicians, and students on board the four cruises are gratefully acknowledged. We also want to thank the two anonymous reviewers, who helped considerably in improving the manuscript. This work was supported by the Netherlands Organization for Scientific Research (NWO), section Earth and Life Sciences (ALW) under grant 854.00.016.

References

Biastoch, A., and W. Krauss (1999), The role of mesoscale eddies in the source regions of the Agulhas current, *J. Phys. Oceanogr.*, *29*, 2303–2317.

Biastoch, A., C. J. C. Reason, J. R. E. Lutjeharms, and O. Boebel (1999), The importance of flow in the Mozambique Channel to seasonality in the greater Agulhas Current system, *Geophys. Res. Lett.*, *26*, 3321–3324.

Biastoch, A., C. W. Boening, and J. Lutjeharms (2008a), Agulhas leakage dynamics affects decadal variability in Atlantic overturning circulation, *Nature*, *456*, 489–492, doi:10.1038/nature07426.

Biastoch, A., J. R. E. Lutjeharms, C. W. Böning, and M. Scheinert (2008b), Mesoscale perturbations control inter-ocean exchange south of Africa, *Geophys. Res. Lett.*, *35*, L20602, doi:10.1029/2008GL035132.

Coward, A. C., and B. A. de Cuevas (2005), The OCCAM 66 level model: Physics, initial conditions and external forcing, *Tech. Rep. 99*, Southampton Oceanogr. Cent., Southampton, U. K.

de Ruijter, W. P., H. Ridderinkhof, J. R. E. Lutjeharms, M. W. Schouten, and C. Veth (2002), Observations of the flow in the Mozambique Channel, *Geophys. Res. Lett.*, *29*(10), 1502, doi:10.1029/2001GL013714.

de Ruijter, W. P. M., H. Ridderinkhof, and M. W. Schouten (2005), Variability of the southwest Indian Ocean, *Philos. Trans. R. Soc. A*, *363*, 63–76.

DiMarco, S. F., P. Chapman, W. D. Nowlin Jr., P. Hacker, K. Donohue, M. Luther, G. C. Johnson, and J. Toole (2002), Volume transport and property distributions of the Mozambique Channel, *Deep Sea Res. Part II*, *49*, 1481–1511, doi:10.1016/S0967-0645(01)00159-X.

Dukowicz, J. K., and R. D. Smith (1994), Implicit free-surface method for the Bryan-Cox-Semtner ocean model, *J. Geophys. Res.*, *99*, 7991–8014.

Ffield, A., J. Toole, and D. Wilson (1997), Seasonal circulation in the South Indian Ocean, *Geophys. Res. Lett.*, *24*, 2773–2776.

Franzese, A. M., S. R. Hemming, and S. L. Goldstein (2009), Use of strontium isotopes in detrital sediments to constrain the glacial position of the Agulhas retroflection, *Paleoceanography*, *24*, PA2217, doi:10.1029/2008PA001706.

Gent, P. R., and J. C. McWilliams (1990), Isopycnal mixing in ocean circulation models, *J. Phys. Oceanogr.*, *20*, 150–155, doi:10.1175/1520-0485.

Godfrey, J. S. (1989), A Sverdrup model of the depth-integrated flow for the world ocean allowing for island circulations, *Geophys. Astrophys. Fluid Dyn.*, *45*, 89–112.

Gordon, A. L. (1986), Interocean exchange of thermocline water, *J. Geophys. Res.*, *91*, 5037–5046.

Griffies, S. M., et al. (2008), Coordinated ocean-ice reference experiments (CORE s), *Ocean Modell.*, *26*, 1–46, doi:10.1016/j.ocemod.2008.08.007.

Harlander, U., H. Ridderinkhof, M. W. Schouten, and W. P. M. de Ruijter (2009), Long-term observations of transport, eddies, and Rossby waves in the Mozambique Channel, *J. Geophys. Res.*, *114*, C02003, doi:10.1029/2008JC004846.

Kistler, R., et al. (2001), The NCEP-NCAR 50-year reanalysis: Monthly means CD-ROM and documentation, *Bull. Am. Meteorol. Soc.*, *82*(2), 247–267.

Large, W. G., J. C. McWilliams, and S. C. Doney (1994), Oceanic vertical mixing: A review and a model with a non-local boundary layer parameterization, *Rev. Geophys.*, *32*(4), 363–403.

Madec, G. (2006), NEMO ocean engine, *Tech. Rep. 27*, Inst. Pierre Simon Laplace, Paris.

Maltrud, M. E., and J. L. McClean (2005), An eddy resolving global 1/10° ocean simulation, *Ocean Modell.*, *8*, 31–54, doi:10.1016/j.ocemod.203.12.001.

Marshall, J., A. Adcroft, C. Hill, L. Perelman, and C. Heisey (1997), A finite-volume, incompressible Navier Stokes model for studies of the ocean on parallel computers, *J. Geophys. Res.*, *102*, 5753–5766.

Matano, R. P., E. J. Beier, P. T. Strub, and R. Tokmakian (2002), Large-scale forcing of the Agulhas variability: The seasonal cycle, *J. Phys. Oceanogr.*, *32*, 1228–1241.

Matano, R. P., E. J. Beier, and P. T. Strub (2008), The seasonal variability of the circulation in the South Indian Ocean: Model and observations, *J. Mar. Syst.*, *74*(1–2), 315–328, doi:10.1016/j.jmarsys.2008.01.007.

Menemenlis, D., I. Fukumori, and T. Lee (2005), Using Green's functions to calibrate an ocean general circulation model, *Mon. Weather Rev.*, *133*, 1224–1240.

Pacanowski, R. C., and S. M. Griffies (1999), The MOM 3 manual, *Tech. Rep. 4*, 680 pp., Natl. Oceanic Atmos. Admin., Princeton, N. J.

Penduff, T. (2005), DRAKKAR: Hiérarchie de modèles glace-océan pour l'étude du climat, *Lett. Trimest. Mercator Océan*, *16*, 2–3.

Quadfasel, D. R., and J. C. Swallow (1986), Evidence for 50-day period planetary waves in the South Equatorial Current of the Indian Ocean, *Deep Sea Res.*, *33*, 1307–1312.

Redi, M. H. (1982), Oceanic isopycnal mixing by coordinate rotation, *J. Phys. Oceanogr.*, *12*, 1154–1158, doi:10.1175/1520-0485.

Ridderinkhof, H., and W. P. M. de Ruijter (2003), Moored current observations in the Mozambique Channel, *Deep Sea Res. Part II*, *50*, 1933–1955.

Ridderinkhof, H., et al. (2010), Seasonal and interannual variability in the Mozambique Channel from moored current observations, *J. Geophys. Res.*, doi:10.1029/2009JC005619, in press.

Rouault, M., P. Penven, and B. Pohl (2009), Warming in the Agulhas Current system since the 1980's, *Geophys. Res. Lett.*, *36*, L12602, doi:10.1029/2009GL037987.

Sasaki, H., M. Nonaka, Y. Masumoto, Y. Sasai, H. Uehara, and H. Sakuma (2008), An eddy-resolving hindcast simulation of the quasiglobal ocean from 1950 to 2003 on the Earth Simulator, in *High Resolution Numerical Modelling of the Atmosphere and Ocean*, edited by K. Hamilton and W. Ohfuchi, chap. 10, pp. 157–185, Springer, New York.

Schott, F., M. Fieux, J. Kindle, J. Swallow, and R. Zantopp (1988), The boundary currents east and north of Madagascar: 2. Direct measurements and model comparisons, *J. Geophys. Res.*, *93*, 4963–4974.

Schott, F. A., and J. P. McCreary (2001), The monsoon circulation of the Indian Ocean, *Prog. Oceanogr.*, *51*, 1–123.

Schott, F. A., S.-P. Xie, and J. P. McCreary Jr. (2009), Indian Ocean circulation and climate variability, *Rev. Geophys.*, *47*, RG1002, doi:10.1029/2007RG000245.

Schouten, M. W., W. P. M. de Ruijter, and P. J. van Leeuwen (2002), Upstream control of Agulhas Ring shedding, *J. Geophys. Res.*, *107*(C8), 3109, doi:10.1029/2001JC000804.

Schouten, M. W., W. P. M. de Ruijter, P. J. van Leeuwen, and H. Ridderinkhof (2003), Eddies and variability in the Mozambique Channel, *Deep Sea Res. Part II*, *50*, 1987–2003.

Smith, R. D., M. E. Maltrud, F. O. Bryden, and M. W. Hecht (2000), Numerical simulation of the North Atlantic Ocean at 1/10°, *J. Phys. Oceanogr.*, *30*, 1532–1561.

Swallow, J., M. Fieux, and F. Schott (1988), The boundary currents east and north of Madagascar: 1. Geostrophic currents and transports, *J. Geophys. Res.*, *93*, 4951–4962.

Uppala, S. M. (2005), The ERA-40 re-analysis, *Q. J. R. Meteorol. Soc.*, *131*(612), 2961–3012, doi:10.1256/qj.04.176.

van Sebille, E., A. Biastoch, P. J. van Leeuwen, and W. P. M. de Ruijter (2009), A weaker Agulhas Current leads to more Agulhas leakage, *Geophys. Res. Lett.*, *36*, L03601, doi:10.1029/2008GL036614.

Webb, D. J., B. A. de Cuevas, and A. C. Coward (1998), The first main run of the OCCAM global ocean model, *Tech. Rep. 34*, Southampton Oceanogr. Cent., Southampton, U. K.

W. P. M. de Ruijter, P. M. van der Werf, and P. J. van Leeuwen, Institute for Marine and Atmospheric Research Utrecht, Department of Physics and Astronomy, Utrecht University, Princetonplein 5, NL-3584 CC Utrecht, Netherlands. (p.m.vanderwerf@uu.nl)

H. Ridderinkhof, Royal Netherlands Institute for Sea Research, PO Box 59, NL-1790 AB Texel, Netherlands.